African Multidisciplinary
Journal of Sciences and Artificial Intelligence

ISSN : 0000-0000

Index: Harvard, Boston, Sydney University, Dimensions, Lens, ResearchGet Scilit, Semantic, Google Scholar, Base etc

https://doi.org/10.58578/AMJSAI.v1i1.3391

NMR Study of Photo-Oxidation of Styrene

Emmanuel Alhassan Kamba & Emmanuel Baaku Attah Daniel
Federal University Wukari, Nigeria
eacambah@gmail.com

Article Info:

Submitted:	Revised:	Accepted:	Published:
Jun 17, 2024	Jul 12, 2024	Jul 14, 2024	Jul 18, 2024

Abstract

In this study, CeO_2 and several Co metal ions doped CeO_2 were synthesized through hydrothermal method and tested for photocatalyzed oxidation of styrene. The characterization data obtained on XRD, EDX and SEM showed the formation process of the synthesized nanoparticles of various sizes as well as the structure of the crystals. Catalyst immobilization technique was utilized to perform a "*pseudo*" *in-situ* photo-oxidation of styrene using NMR spectroscopy. Using molecular oxygen as the oxidant, 0.3 mol % Co-doped CeO_2 showed the highest conversion of 45 % while the selectivities for styrene oxide and benzaldehyde were 38 % and 51 % respectively. As revealed by the kinetic study in this work, the photo-oxidation reaction proceeded according to Langmuir-Hinshelwood model. The synthesized catalyst showed high stability and reusability over several photo-oxidation cycles. CeO_2 is indeed a promising catalyst ideal for photo-oxidation reactions to produce styrene oxide.

Keywords: Photocatalyst, Styrene, Styrene-oxide, Cerium-dioxide

INTRODUCTION

As the demand for new techniques for screening semiconductor photo-catalysts keep rising, a significant amount of research into this field are also increasing. The use of oxides of rare-earth metals is yet another significant area that has received much attention due to the attractive properties such as optical and magnetic properties [1] of these materials. This group of materials has also demonstrated appreciable catalytic properties. One of the highly studied is cerium oxide (CeO_2). CeO_2 is one of the widely used rare-earth metal oxides that has gained the attention of the academia and industry for decades [2]. Some of its advantages include the Ce^{3+}/Ce^{4+} reduction-oxidation cycle as well as the ability to store oxygen, otherwise known as Oxygen Storage Capability (OSC). The oxidative properties of CeO_2 is dependent on the reduction step between Ce^{3+} and Ce^{4+} also referred to as the Ce^{3+}/Ce^{4+} redox cycle [2-4]. This property is mainly caused by its high reduction potential as well as the OSC, the extent of which is a function of the size, morphology, shape as well as surface area of the material. At an average size between 10 and 15 nm, CeO_2 nanomaterial exhibits a phenomenon known as quantum confinement effect [3]. They also exhibit an appreciable growth of cell parameters owing to the oxygen vacancies present as a result of the increase in number of Ce^{3+}. It has been reported that due to enhancement of the ratio of Ce^{3+} to Ce^{4+}, the OSC can be improved by coupling CeO_2 with ions of a transition metal or another rare-earth metal [5]. Higher surface energy also plays a crucial role in the enhancement of the material's activity, as it is responsible for the improved activity of the observed (100) surface of cubic CeO_2. In descending order, the surface energy of cubic CeO_2 is as follows: (100) > (110) > (111) [6]. The ability to control some of the most desirable properties of CeO_2 nanostructures has justified their interest over the conventional aggregated nanoparticles. Some of these physicochemical properties include architecture, morphology and growth direction. There exist several morphologies of CeO_2 nanostructures in the literature. Among these, one-dimensional nanorods, aggregates, and wires have drawn a lot of attention owing to their high specificity of both surface area and active crystallography in the direction of growth [6-9]. However, only the aggregate morphology was synthesised in the work due to its certain advantages that have been outlined in the literature. Due to its porous structure and high surface area an enhanced contact between the catalyst and the substrate can be achieved. Moreover, a significant decrease in sintering could be achieved due to the porosity created when aggregates are stacked randomly [7]. Effectively, decreasing sintering leads to sustenance of surface area

which otherwise would be reduced at higher temperature. One of the methods for synthesising aggregate CeO_2 is the hydrothermal method. However, in order to achieve precision in width size, aspect ratio as well as accessible surface active sites, a lot is still required to be done. Nevertheless, high level of control could be achieved when a suitable precursor, a suitable reaction medium and conditions are carefully chosen.

Styrene epoxidation reaction is one of the most important chemical reactions in the chemical industry. Due to its commercial value, styrene oxide is extensively used as an intermediate for production of variety of pharmaceutical and fine chemical products. It is normally synthesised using two principal methods. The first is the use of a suitable base to de-hydrochlorinate styrene chlorohydrin while the second method involves the use of H_2O_2, organic peracids or urea-H_2O_2 to oxidise styrene [8-10]. Unfortunately, neither of these methods is environmentally or economically friendly due to the use of hazardous chemical substances. In order to synthesise styrene oxide in a "greener" way, the use of heterogeneous photo-catalyst and molecular oxygen could be employed for the oxidation reactions. In spite of the efficiency of CeO_2 as a catalyst, only a few reports have been made about it.

In this study, hydrothermal method was utilised to synthesise CeO_2 and Co metal ion doped CeO_2 nanostructured photo-catalyst. NMR screw cap tube was utilized as the reaction vessel which allowed for the use of economical quantities (1 mL) of reactants. This novel technique is a possible quick technique for screening of a variety of organic reactions.

METHODS

Experimental Procedure

All reagents used in this study were used as supplied. No further treatment was performed on any chemical.

Preparation of CeO_2 catalyst

Hydrothermal method was used to synthesise CeO_2 aggregate. 1 g of cerium (III) nitrate hexahydrate ($Ce(NO_3)_3{\cdot}6H_2O$) was pre-mixed with 10 mL ethylene glycol. 0.3 M ammonium hydroxide was added dropwise until a pH of 7 was achieved. A straw yellow mixture was obtained which was stirred vigorously for 3 h. The final mixture was transferred to a Teflon vessel and an autoclave, placed in an oven for hydrothermal

synthesis at 120 °C for 24 h. When the autoclaves have cooled down to room temperature, the formed precipitates were separated by centrifuging and vacuum filtering, washed thoroughly with de-ionised water followed by ethanol and dried at 80 °C for 12 h. The final dried powder was then calcined at 500 °C for 6h.

For preparation of Co doped CeO_2, 1 g of $Ce(NO_3)_3{\cdot}6H_2O$ was pre-mixed with 10 mL ethylene glycol. 0.2 g of cobalt (II) nitrate hexahydrate ($Co(NO_3)_2{\cdot}6H_2O$, 97.5 %) was dissolved in 15 mL ethanol and added to the first mix under magnetic stirring. The next steps from addition of 0.3 M ammonium hydroxide to calcination, were as above.

The same general procedure as above was followed for preparing different mol ratio of cobalt metal ion doped-CeO_2. The various doping amount and their allocated names in the study are displayed on Table 1.

Table 1: Amount of Co in Co doped-CeO_2

Entry	Amount (mol %)	Thesis allocated name
1	0.0	CeO_2
2	0.1	Co(0.1)-CeO_2
3	0.3	Co(0.3)-CeO_2
4	1.0	Co(1.0)-CeO2

Preparation of catalyst loaded NMR Tubes

Using a novel technique, NMR screw cap tube was used as the reactor. Catalysts synthesised in section 2.1, were individually immobilised on glass beads by spinning appropriate amount of catalyst and the beads in a plastic bottle (200 mL) on a spinner. This was then placed in a 600 MHz frequency, 7 in. and 5 mm outer diameter screw cap NMR tube. A piece of quartz wool was placed before the catalyst coated beads to keep the latter from falling to the lower part of the tube as doing so may obstruct the NMR reading as seen in the set-up shown in Figure 1 (left).

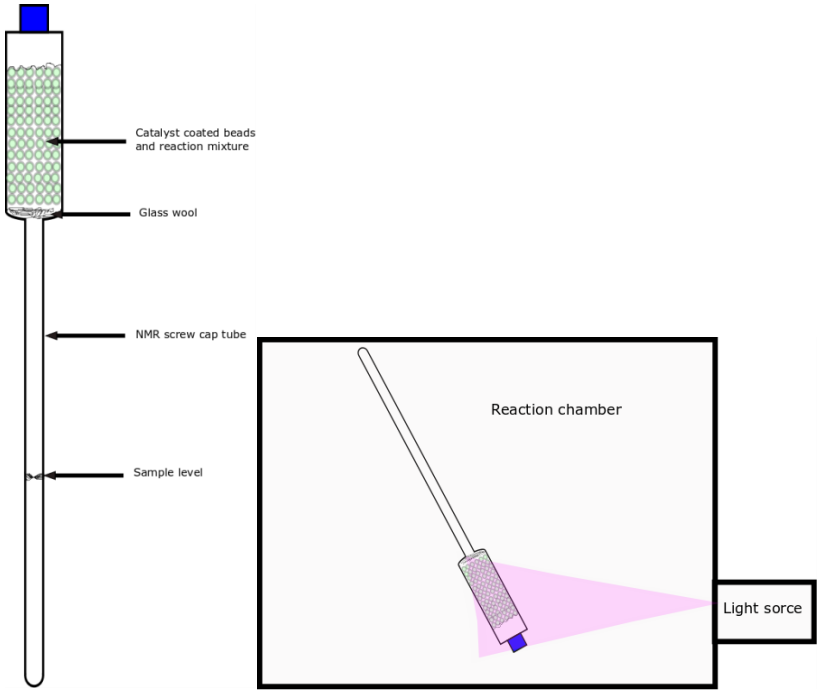

Figure 1: ***NMR tube assembly (left); reaction set-up (right)***

Styrene catalytic oxidation reaction

When the reactor in Figure 1 was ready for reaction, the reactants were added as follows: separately, 1.5 mL of chloroform-d was placed in a GC autosampling vial and 20 uL of styrene was added and thoroughly shaken to homogeneity. The solution was then transferred to the NMR tube assembly with the aim of a syringe. A bleed needle was inserted through the septum on the screw cap to reduce pressure build-up during this process. 5 mL of molecular oxygen was also pumped into the reaction set-up as the oxidant. The tube was then inverted to allow contact between the reacting species and placed in a crosslinker UV chamber and irradiated with 2.0 $mWcm^{-2}$ of light from a xenon light source as shown in Figure 1 (right). NMR analysis was performed periodically after every 10 min of illumination by taking the reactor and keeping it vertical for a couple of minutes to allow the liquid drain to the bottom of the tube, then placed in a 600 MHz Varian NMR. This was repeated until no further changes in the NMR spectra was observed. The cycle was performed for all the catalysts.

RESULTS AND DISCUSSION

XRD analysis

The XRD patterns of the CeO_2 nanoparticles are shown in Figure 2. A well resolved diffraction peaks for CeO_2 corresponding to a standard data JCPDS 34-0394 can be seen.

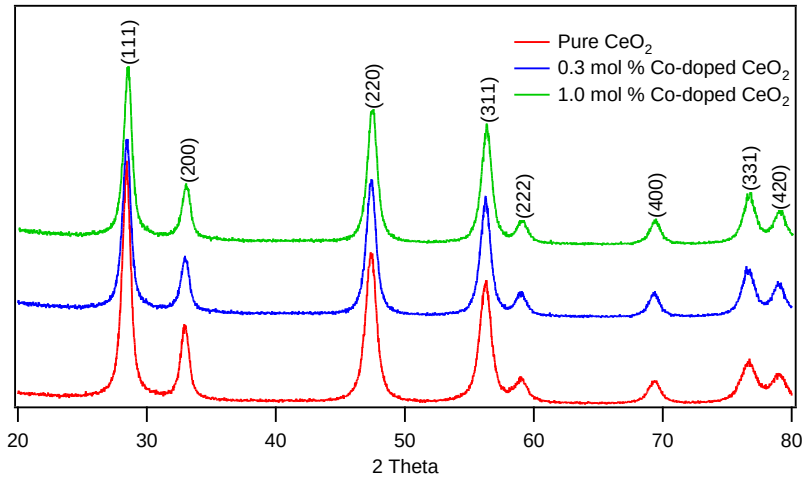

Figure 2: ***Powder XRD patterns of synthesized pure and cobalt impregnated CeO_2 NP***

No observation was made for peaks associated with cerium hydroxide. This suggests the direct formation of crystalline CeO_2 particles from the cerium nitrate precursor solution. Interestingly, the peaks intensity ratio of 0.5 was achieved for the (200) and (220) crystals of CeO_2 nanoparticles. Ideally, the peaks intensity ratio should be 0.6 [11]. This observation shows specificity in the growth direction of the crystals of the CeO_2 nanoparticles synthesised and is well documented in the literature [12-15]. Using Scherer's Equation, it was possible to determine the average sizes of the crystallites considering the broadness of the diffraction peak (111). As the calcination temperature was increased the average crystallite sizes also increased as displayed on Table 2. It can also be seen on Table 2 that the crystals of the CeO_2 nanoparticles synthesised were longer than those of bulk CeO_2. This is consistent with the findings of Pal et al. which they attributed to be due to grain surface relaxation (that plays a vital role in the line broadening which results in reduction of the dislocation density) [16] as well as the presence of Ce^{3+}, which leads to a high redox potential of CeO_2 nanocrystals.

Table 2: ***The crystallinity and unit cell parameters of the synthesised catalysts***

Entry	Sample	S_{BET} (m^2g^{-1})	Crystallite size (nm)
1	CeO_2	47.21	6.28
2	Co(0.1)-CeO_2	52.47	7.45
3	Co(0.3)-CeO_2	51.41	7.78
4	Co(1.0)-CeO_2	64.12	7.86

As Ce^{4+} is being replaced with Ce^{3+}, due to the higher atomic radii of Ce^{3+} an enhancement of the crystal lattice of the CeO_2 nanoparticles can be observed according to Vegard's rule. The XRD patterns of Co–CeO_2 (Figure 2) was not different from that of pure CeO_2 as expected, since dopants usually have no effect on XRD pattern [17]. There was no additional peak corresponding to cobalt oxide even though the catalyst was calcined at 500 ^oC. This can be attributed to the low amount of the material present in the final Co-CeO_2 material. Another possible reason is that the Co was uniformly dispersed in the overall material.

SEM Analysis

The synthesised CeO_2 and its dopants were further characterised by SEM as shown in Figure 3. The SEM images of the CeO_2 show an irregular shaped material of micro-meter length. The observed morphology of CeO_2 did not show any significant change with calcination. Similarly, due to low amount of dopant used in the syntheses of Co doped CeO_2 no difference was observed in the morphology of the base CeO_2. As such, EDX analysis was performed to ascertain the presence of Co ions in the finished material (Figure 4). The elemental composition data on Table 8.1 shows the presence Co up to 0.5 wt % with 0.44 at %.

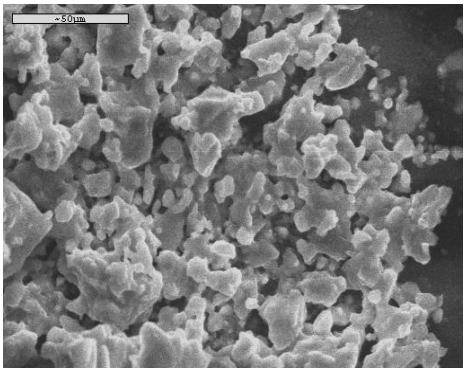

Figure 3: ***SEM images of as-synthesized CeO_2***

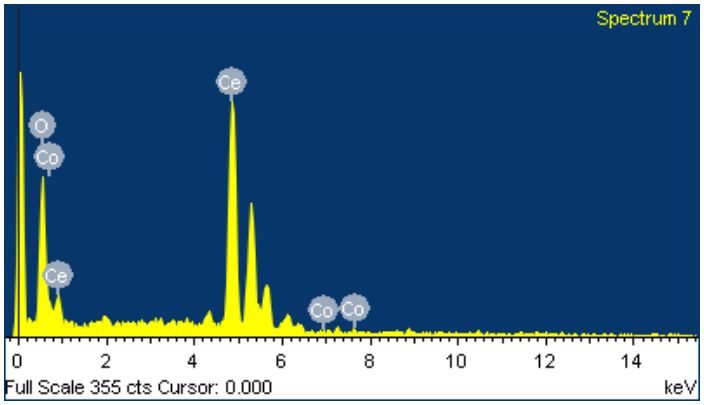

Figure 4: ***EDX spectrum of 0.3 mol % Co-CeO_2***

Conventionally, synthesis of CeO_2 nanoparticles is performed through the formation of cerium carbonate or hydroxide intermediate which often result in low formation of product and is not time efficient [18-21]. Here, a direct formation procedure was adopted by using cerium (III) nitrate hexahydrate which under hydrothermal condition nucleates to form CeO_2 nanoparticles during the initial reaction. Ethylene glycol also played a vital role in CeO_2 particles formation as it provided a platform upon which the CeO_2 particles grew. Ethylene glycol has been reported to play a role in morphology control as well as crystal growth direction [22]. Wang et al. [23] explained that when poly ethylene glycol is used, at the initial stage of CeO_2 growth mechanism, nanoparticles independently arrange themselves in such a way that their crystallographic orientation is the same. After that, the particles combine at a planar interface that result in a decrease in the surface energy. As also observed by Pal et al. the (100) corresponds to the binding of the nanoparticles on the chains of poly ethylene glycol which led to surface energy reduction. This was followed by the enlargement of the particle and eventual oriental attachment on the next available reactive surface (110) [24]. Upon poly ethylene glycol removal, (100), which is the highly energetic surface became highly exposed. On the other hand, when ethylene glycol is used, the particles tend to form an agglomerate by dehydrating and then condensing to form particles with an irregular shape due to the presence of hydroxyl group on the CeO_2 surface. This explain the morphology of the CeO_2 nanoparticles obtained in this work.

Catalytic activity study

Analysis was carried out to study the photo activities of the synthesised catalysts by plotting the concentration profile of styrene as well as those of styrene oxide and benzaldehyde.

This data was generated by taking 2 µl of the NMR reaction tube after each round of illumination, using a micro syringe. The eluent was injected in to GCMS and corresponding peak of species were analysed. It can be seen from the GCMS data in Figure 5 that all the catalysts were active toward photooxidation of styrene. Figure 5 (A) shows the normalised styrene concentration data according to catalysts and time of reaction.

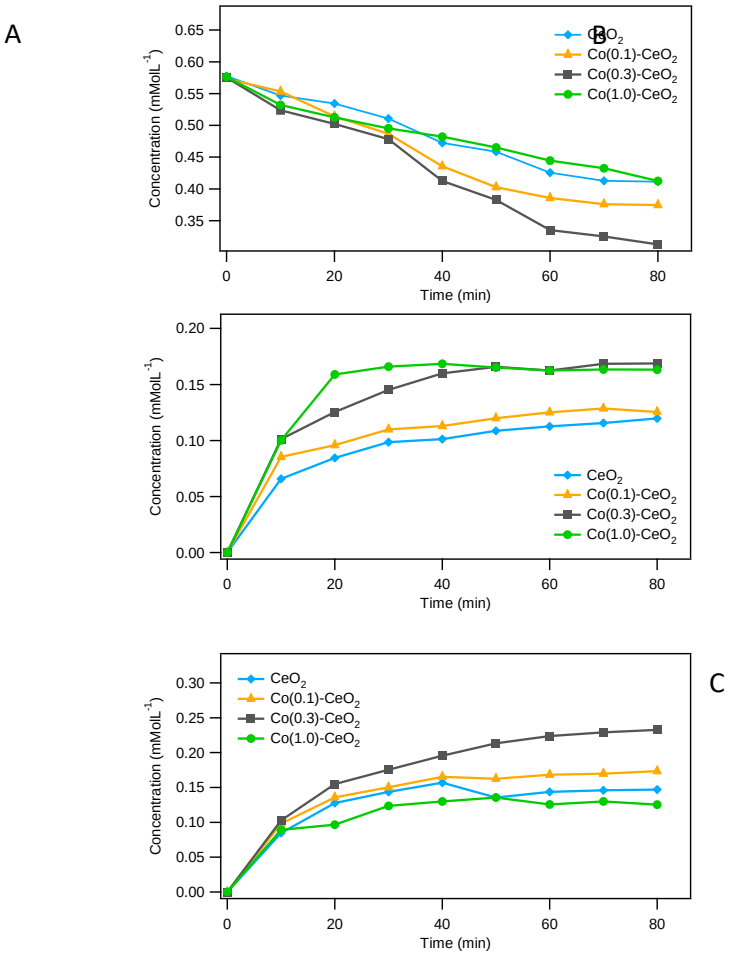

Figure 5: ***Concentration profile for styrene (A), styrene oxide (B) and benzaldehyde (C) obtained for the oxidation of styrene with O_2 over all the synthesized CeO_2 based catalysts.***

It can be seen here that the highest decrease in styrene concentration which corresponds to conversion of 45 % was achieved with Co(0.3)-CeO_2. However, the highest increase in concentrations of styrene oxide was achieved with Co(1.0)-CeO_2 which corresponds to selectivity of 61%. These modified CeO_2 catalysts performed better than pure CeO_2 with respect to conversion and selectivity.

The incorporation of cobalt to the CeO_2 catalyst showed an improved activity which can be attributed to an increase in the sites vacancies as a result of enhanced number of Ce^{3+} ions which in turn increases the number of active sites to adsorb more oxygen molecules [25]. On the other hand, increasing the amount of Co to make 1.0 mol % Co-CeO_2, showed a decrease in conversion of styrene and selectivity of benzaldehyde. This is probably due excess un-bonded Co ions which could cause surface deactivation [26]. Nevertheless, pure CeO_2 achieved the lowest conversion and selectivity showing clearly the superiority of Co impregnated CeO_2, which is most likely due to three major factors: increased surface area, increased number of Ce^{3+} ions as well as revealed surface of active (100) [24-27]. This observation is in agreement with the literature.

NMR Analysis

Figure 6 represents the distribution and allocation of protons according to their electronic environments. The position of a proton on the structure determines whether its peak will appear at a high or low shift relative to a reference. The number of peaks in the NMR spectrum is equal to the number of protons (or other atoms) in the molecule. Also the proximity of a proton to an electronegative atom or multiple bond leads to a peak appearing more downfield. Since ^{1}H-NMR spectrum produces peaks according to this classification, it became imperative to identify these individual peaks and their sources from the three major molecules present before (Figure 6 (A)) and after (Figure 6 (B & C)) reaction. Identification of all peaks was further confirmed by considering their multiplicity as well as by comparing with ACD/I-Lab database.

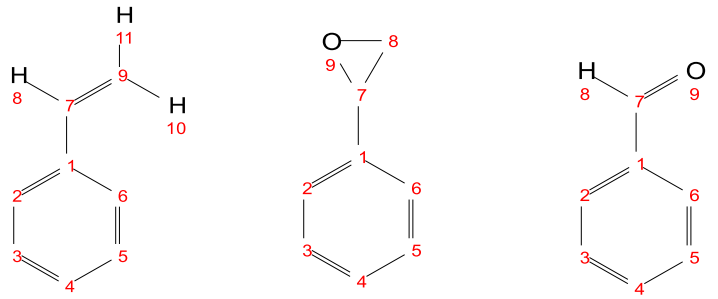

(A) (B) (C)

Figure 6: Schematic representation of electronic environments of H atoms within the molecules of (A) styrene, (B) styrene oxide and (C) benzaldehyde.

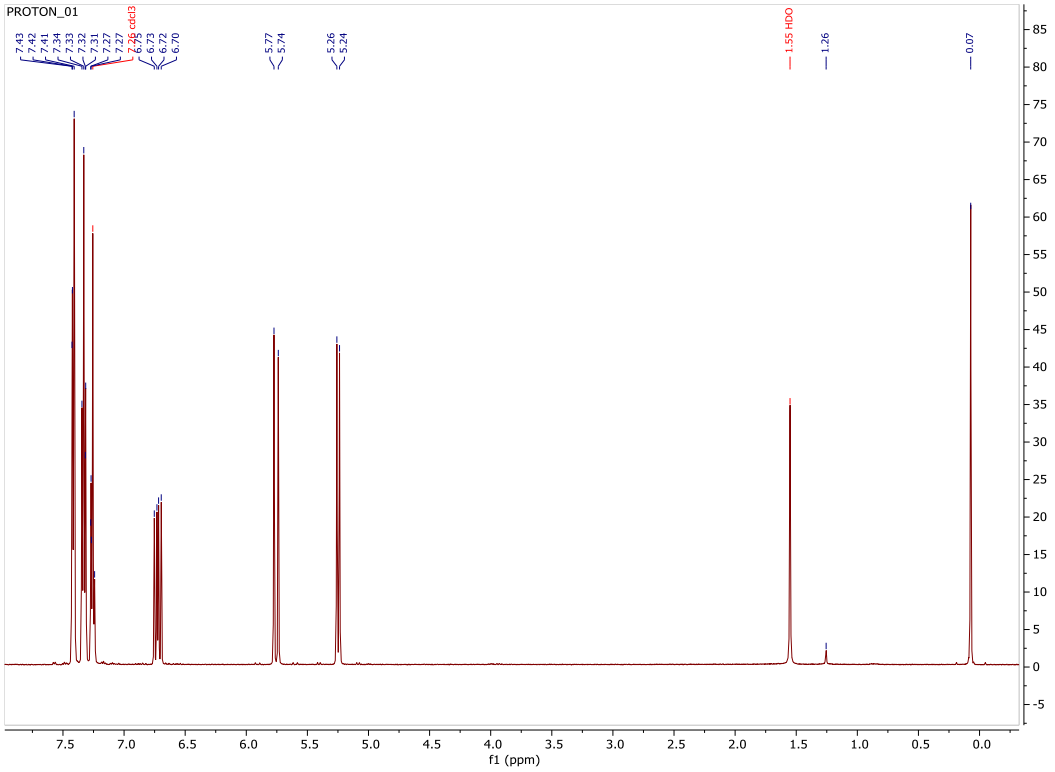

Figure 7: ***^{1}H-NMR of reaction mixture before illumination***

Figure 7 shows the ^{1}H-NMR spectrum of reaction mixture before reaction (irradiation). The peaks at 1.2 and 1.55 ppm are likely due to impurities in the mixture. At 5.2, 5.7 and 6.66 ppm, the peaks correspond to H in the electronic environments labelled 11, 10 and 8 respectively, in Figure 6 (A). The multiplet peak at 7.23 corresponds to the $CDCl_3$. However, several peaks appeared almost overlapping with the solvent peak at 7.23 ppm. These peaks are attributed to the aromatic ring with protons labelled 1 to 6 in Figure 6. After every 10 min of reaction, NMR analysis was performed until no further changes were observed in the NMR spectra. Figure 8 (A) shows the ^{1}H-NMR of photo-reacted styrene using Co(0.3)-CeO_2. As can be seen here, spectrum 7, which is the initial reaction spectrum at time 0 min. shows peaks similar to those in Figure 7. This implies that no reaction took place in the absence of light. After 10 min of reaction, new peaks appeared between 2.0 and 4.0 ppm which were absent before illumination (Figure 8, spectrum 6). Similarly, further downfield at 10.2 ppm another new peak appeared which can be attributed to protons labelled 8 in Figure 6 (C). The downfield appearance of this peak is due to the proximity of the protons to a double bond as well as O (a highly electronegative atom) [28]. This peak has been identified as benzaldehyde.

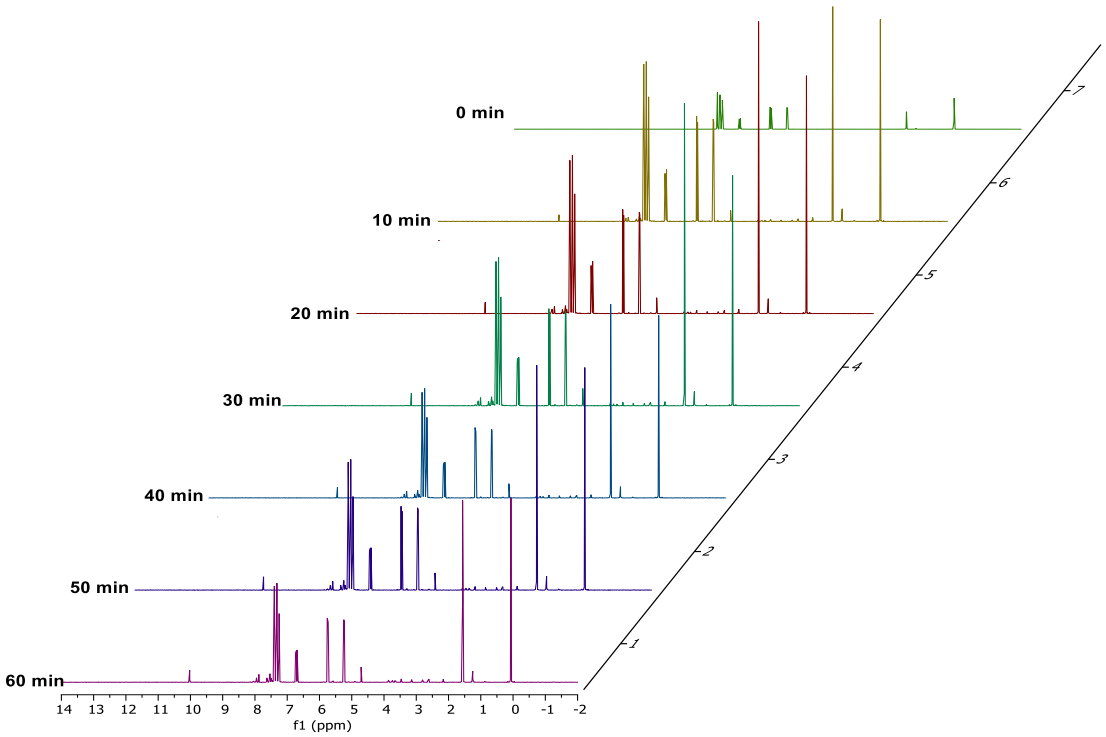

Figure 8: ***Full spectra of ^{1}HNMR of styrene epoxidation after irradiation at 10 min interval for 60 min.***

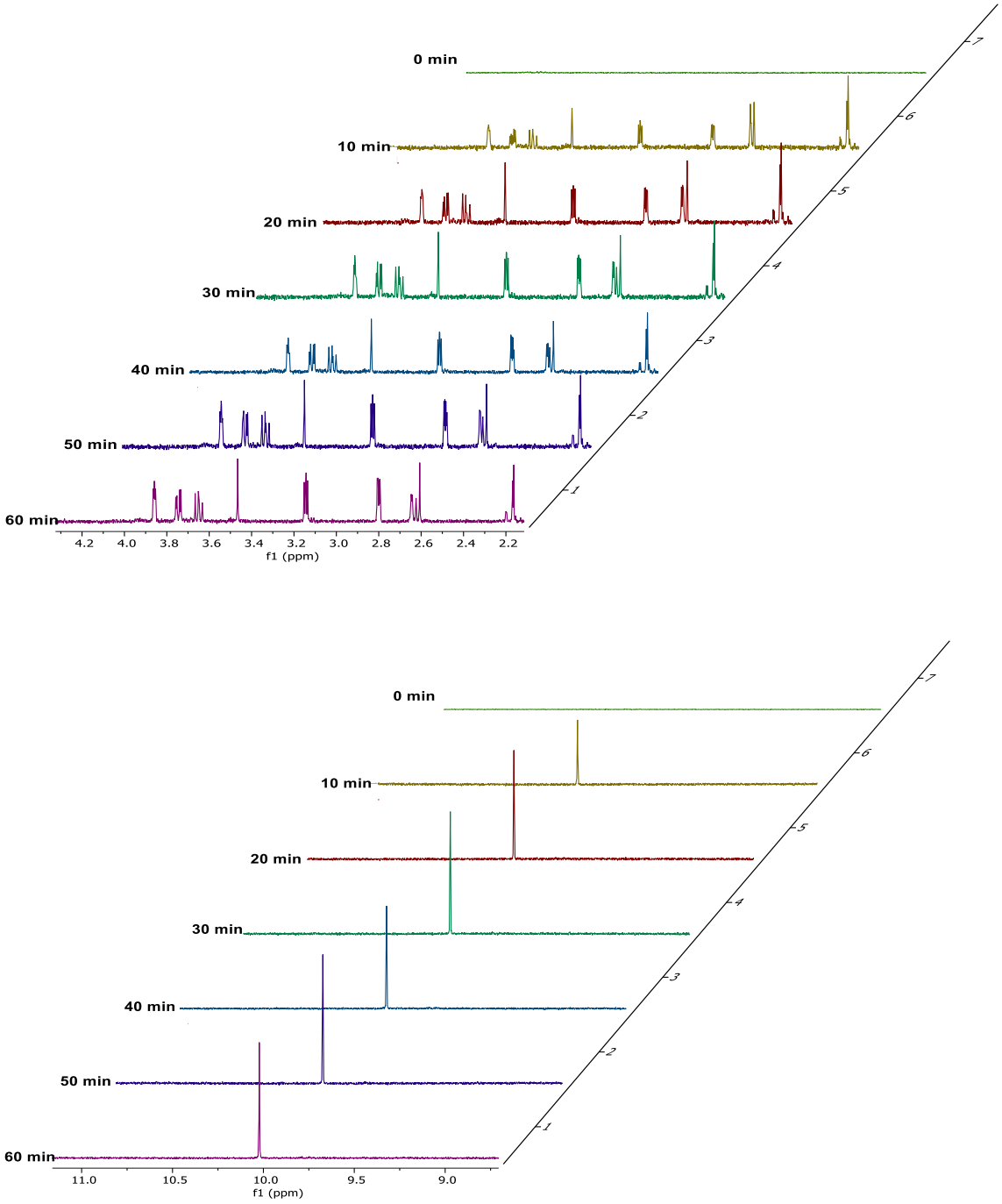

Figure 9: ***Zoomed in ^{1}HNMR of styrene epoxidation showing (A) peaks due to styrene oxide and (B) peak at 10.2 ppm, due to benzaldehyde***

From Figure 9 (A), the emergence of new peaks after reaction can be seen. All the peaks which were absent at 0 min reaction time, appeared after 10 min of reaction. No other different peaks were observed after this time. This shows that only one type of reaction occurred in the system and the products did not suffer any form of decomposition. The emerged peaks were also observed to retain their intensity between 20 and 60 min of reaction. Only a slight increase in intensity was observed from 10 min to 20 min of reaction, which can be ascribed to initial product formation process. Similarly, the proton peak at 10.2 ppm remained stable within the reaction period tested (Figure 9 B). Figure 10 shows peaks at 2.80, 3.15 and 3.86 ppm which have been ascribed to protons of styrene oxide in chemical environments labelled 8, 8 and 7 respectively. These were identified by first stacking the spectrum of a standard styrene oxide with that of reaction after 60 min.

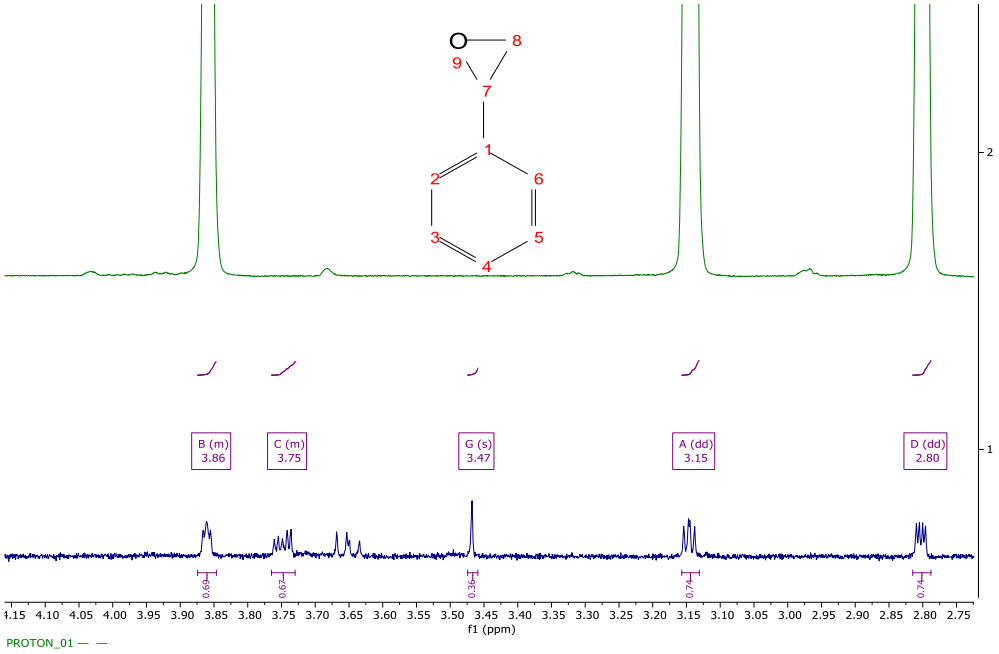

Figure 10: ***Comparison between NMR spectra of standard styrene oxide (green) and reaction product at 60 min (blue).***

The multiplicity of the selected peaks in Figure 10 further confirms the identity of the product. By determining the coupling constant of the selected peaks, it can be seen that peaks at 2.80 and 3.15 ppm are doublets. Also, form the coupling constant, peak at 3.86 ppm is a multiplet. Considering protons at C labelled 8 in the styrene oxide structure, their neighbouring proton at C labelled 7 is 1. As such, applying the *N+1* rule results in 2, hence the doublet peaks observed at 2.80 and 3.15 ppm. Similarly, applying this rule to peak at

3.86 ppm gives a multiplet. Other peaks whose identity could not be confirmed by NMR were also observed. Around 3.47 ppm a singlet, around 3.63 ppm a singlet, around 3.67 ppm a singlet and around 3.75 ppm a multiplet.

Kinetic considerations

The oxidation reaction of styrene can be summarised in Equation (8.1) as follows:

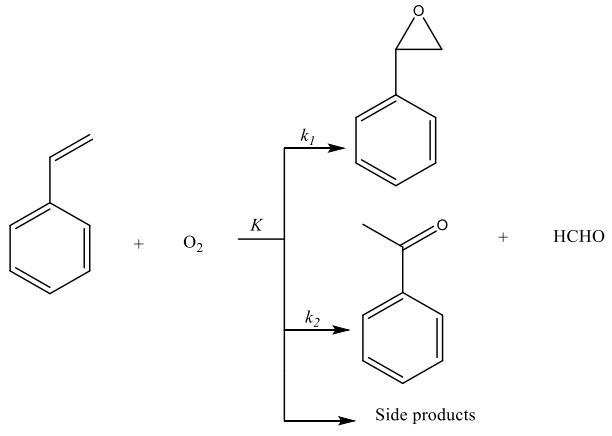

(1)

where the rate constants *K, k_1* and *k_2* were estimated at different reaction temperatures. Using the Arrhenius Equation, $K = Ae^{-Ea/RT}$, the plot of ln K, ln k_1 and ln k_2 against 1/T (Figure 11) showed linear relationships. From these plots, the activation energies for styrene, styrene oxide and benzaldehyde were determined to be 12.87 $kJmol^{-1}$, 8.52 $kJmol^{-1}$ and 11.96 $kJmol^{-1}$,

respectively.

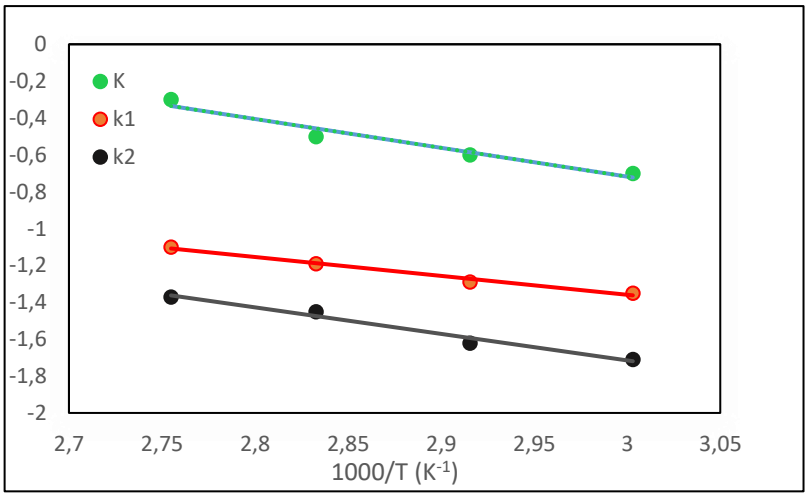

Figure 11: Arrhenius plot of photo oxidation of styrene over Co(0.3)-CeO_2 catalyst.

From the Arrhenius plots, the activation energy of benzaldehyde is greater than that of styrene oxide. This implies that production of benzaldehyde is favoured at higher temperature more than styrene oxide. At lower temperatures, the cleavage of C=C occurred easily while at higher temperatures epoxidation competes more preferentially [29].

The linear relationship obtained in Figure 11 strongly suggests that the photocatalytic oxidation of styrene preformed here using molecular oxygen as the oxidant and CeO_2-based nanoparticles as catalyst proceeded according to Langmuir-Hinshelwood model which means that reaction occurred at the surface between adsorbed styrene and oxygen.

Reaction mechanism

Several possible reaction routes have been proposed for heterogeneous photo-catalysed oxidations in the presence of molecular oxygen, out of which two models are widely used. Mars-van Krevelen and Langmuir-Hinshelwood mechanisms have helped to identify the reaction pathways which is essential in understanding the overall reaction mechanism. According to Mars-van Krevelen model, the oxidation process occurs by loss of O on the surface of catalyst which is then replaced by molecular oxygen. However, the model assumes the reaction can proceed significantly in the absence of O since the lattice O of the catalyst surface is responsible for the reaction. The Langmuir-Hinshelwood model on the other hand describes the reaction where the substrate adsorbed on one site and O adsorbed on a different site of the catalyst react. Since O was an essential reagent in this work as no product was made without it, it is therefore apparent that the photo catalysed oxidation of styrene studied here followed the Langmuir-Hinshelwood model. However, more investigations need to be carried out to confirm this claim.

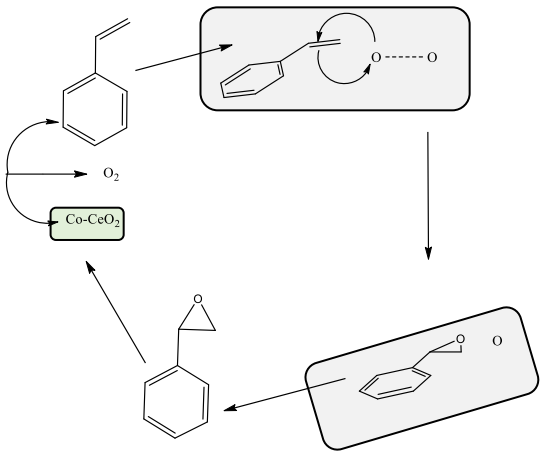

Scheme 1: Proposed probable reaction mechanism of styrene oxidation with O_2 over synthesized CeO_2 NW based catalyst.

Scheme 1 shows a proposed mechanism for the epoxidation reaction of styrene. It starts by adsorbing styrene onto the surface of the catalyst (CeO_2-based nanoparticles) as a result of p-interaction associated with aromatic ring [30]. Then follows the adsorption of oxygen onto the surface of the catalyst. On the surface of the CeO_2 nanoparticles, some sites become vacant as a result of the formation of Ce^{3+}. It is these vacancies that are occupied by molecular oxygen [31]. Eventually, the adsorbed species (styrene and oxygen) interact together to form the product styrene oxide. The other oxygen atom is left to either interact with Ce^{3+} and participate in the redox cycle or interact with another molecule of styrene.

CONCLUSION

In this study, another application of the catalyst coating technique has been demonstrated. CeO_2 and Co-CeO_2 nanoparticles were successfully synthesised, characterised and tested for photocatalytic oxidation of styrene. The nanoparticles powder with highly exposed active (100) surface were coated on glass beads and placed in an NMR tube to make a simple photo reactor. In order to improve the efficiency of CeO_2 nanoparticles in photo-oxidation of styrene, different amounts of Co ions were added as dopant owing to the wide knowledge of Co complexes as efficient catalysts for selective oxidation of alkenes [32].

The photo catalytic experimental results showed that the catalysts have high activity towards oxidation of styrene using molecular oxygen as oxidant. Co(0.3)-CeO_2 showed the highest conversion of styrene peaking at 45% while the highest selectivity of 61 % for styrene oxide was obtained with Co(1.0)-CeO_2. The kinetic study performed revealed that

the reaction agrees with Langmuir-Hinshelwood model based on which a proposal for the possible reaction mechanism was made. The technique developed in this work can serve as a quick screening technique for both catalysts and oxidation of organic materials in the presence of molecular oxygen.

Conflict of Interest

The authors declare that they have no conflict of interest.

REFERENCES

[1] R. Si, Y. W. Zhang, L. P. You and C. H. Yan, Rare-earth oxide nanopolyhedra, nanoplates, and nanodisks, *Angew. Chemie - Int. Ed.*, 2005, **44**, 3256–3260.

[2] W. Zhu, K. Tang, J. Li, W. Liu, X. Niu, G. Zhao, X. Ma, Z. Liu, H. Wei and Y. Yang, The effect of copper species in copper-ceria catalysts: structure evolution and enhanced performance in CO oxidation, *RSC Adv.*, 2016, **6**, 46966–46971.

[3] D. C. Sayle, S. A. Maicaneanu and G. W. Watson, Atomistic Models for CeO_2 (111), (110), and (100) Nanoparticles, Supported on Yttrium-Stabilized Zirconia, *J. Am. Chem. Soc.*, 2002, **124**, 11429–11439.

[4] Y. Shao and Y. Ma, Mesoporous CeO_2 nanowires as recycled photocatalysts, *Sci. China Chem.*, 2012, **55**, 1303–1307.

[5] H. De Lasa, B. Serrano and M. Salaices, *Photocatalytic reaction engineering*, 2005.

[6] M. Obst and B. König, Solvent-free, visible-light photocatalytic alcohol oxidations applying an organic photocatalyst, *Beilstein J. Org. Chem.*, 2016, **12**, 2358–2363.

[7] G. Jones, Origin of catalytic activity in sponge Ni catalysts for hydrogenation of carbonyl compounds, *Catal. Struct. React.*, 2015, **1**, 78–87.

[8] X. Li, Y. Li, Y. Huang, T. Zhang, Y. Liu, B. Yang, C. He, X. Zhou and J. Zhang, Organic sponge photocatalysis, *Green Chem.*, 2017, **19**, 2925–2930.

[9] Y. Kanda, A. Seino, T. Kobayashi, Y. Uemichi and M. Sugioka, Catalytic Performance of Noble Metals Supported on Mesoporous Silica MCM-41 for Hydrodesulfurization of Benzothiophene, *J. Japan Pet. Inst.*, 2009, **52**, 42–50.

[10] R. K. Liew, M. Y. Chong, O. U. Osazuwa, W. L. Nam, X. Y. Phang, M. H. Su, C. K. Cheng, C. T. Chong and S. S. Lam, Production of activated carbon as catalyst support by microwave pyrolysis of palm kernel shell: a comparative study of chemical versus physical activation, *Res. Chem. Intermed.*, 2018, **44**, 3849–3865.

[11] M. A. Henderson, Effect of coadsorbed water on the photodecomposition of acetone on TiO_2 (110), *J. Catal.*, 2008, **256**, 287–292.

[12] L. Liu, H. Zhao, J. M. Andino and Y. Li, Photocatalytic CO_2 Reduction with H_2O on TiO_2 Nanocrystals: Comparison of Anatase, Rutile, and Brookite Polymorphs and Exploration of Surface Chemistry, *ACS Catal.*, 2012, **2**, 1817–1828.

[13] T. Li, W. Zeng, H. Long and Z. Wang, Nanosheet-assembled hierarchical SnO_2 nanostructures for efficient gas-sensing applications, *Sensors Actuators, B Chem.*, 2016, **231**, 120–128.

[14] J. He, Q. Zhai, Q. Zhang, W. Deng and Y. Wang, Active site and reaction mechanism for the epoxidation of propylene by oxygen over CuO_x/SiO_2 catalysts with and without Cs+ modification, *J. Catal.*, 2013, **299**, 53–66.

[15] M. El-Maazawi, A. N. Finken, A. B. Nair and V. H. Grassian, Adsorption and Photocatalytic Oxidation of Acetone on TiO_2: An in Situ Transmission FT-IR Study, *J. Catal.*, 2000, **191**, 138–146.

[16] H. Song, Y. Li, Z. Lou, M. Xiao, L. Hu, Z. Ye and L. Zhu, Synthesis of Fe-doped WO_3 nanostructures with high visible-light-driven photocatalytic activities, *Appl. Catal. B Environ.*, 2015, **166–167**, 112–120.

[17] C. Raillard, V. Héquet, P. Le Cloirec and J. Legrand, Kinetic study of ketones photocatalytic oxidation in gas phase using TiO_2-containing paper: effect of water vapor, *J. Photochem. Photobiol. A Chem.*, 2004, **163**, 425–431.

[18] N. L. Nagda and H. E. Rector, A critical review of reported air concentrations of organic compounds in aircraft cabins, *Indoor Air*, 2003, **13**, 292–301.

[19] A. Fujishima, T. N. Rao and D. A. Tryk, Titanium dioxide photocatalysis, *J. Photochem. Photobiol. C Photochem. Rev.*, 2000, **1**, 1–21.

[20] J. J. Testa, M. A. Grela and M. I. Litter, Experimental evidence in favor of an initial one-electron-transfer process in the heterogeneous photocatalytic reduction of chromium(VI) over TiO_2, *Langmuir*, 2002, **17**, 3515–3517.

[21] R. Mu, Z. Xu, L. Li, Y. Shao, H. Wan and S. Zheng, On the photocatalytic properties of elongated TiO_2 nanoparticles for phenol degradation and Cr(VI) reduction, *J. Hazard. Mater.*, 2010, **176**, 495–502.

[22] T. T. Y. Tan, C. K. Yip, D. Beydoun and R. Amal, Effects of nano-Ag particles loading on TiO2 photocatalytic reduction of selenate ions, *Chem. Eng. J.*, 2003, **95**, 179–186.

[23] S. Wang, Z. Ding and X. Wang, A stable $ZnCo_2O_4$ cocatalyst for photocatalytic CO_2 reduction, *Chem. Commun.*, 2015, **51**, 1517–1519.

[24] T. Inoue, A. Fujishima, S. Konishi and K. Honda, Photoelectrocatalytic reduction of carbon dioxide in aqueous suspensions of semiconductor powders, *Nature*, 1979, **277**, 637–638.

[25] D. Li, X. Fang, H. Liu, H. Lu and Z. Zhang, in *AIP Conference Proceedings*, AIP Publishing LLC , 2018, vol. 1971, p. 020006.

[26] A. Kumar, A Review on the Factors Affecting the Photocatalytic Degradation of Hazardous Materials, *Mater. Sci. Eng. Int. J.*, , DOI:10.15406/mseij.2017.01.00018.

[27] H. Ghafarian-Zahmatkesh, M. Javanbakht and M. Ghaemi, Ethylene glycol-assisted hydrothermal synthesis and characterization of bow-tie-like lithium iron phosphate nanocrystals for lithium-ion batteries, *J. Power Sources*, 2015, **284**, 339–348.

[28] T.-D. Nguyen-Phan and E. W. Shin, Morphological effect of TiO_2 catalysts on photocatalytic degradation of methylene blue, *J. Ind. Eng. Chem.*, 2011, **17**, 397–400.

[29] L. Lopez, W. A. Daoud, D. Dutta, B. C. Panther and T. W. Turney, Effect of substrate on surface morphology and photocatalysis of large-scale TiO2 films, *Appl. Surf. Sci.*, 2013, **265**, 162–168.

[30] C. Adán, J. Marugán, E. Sánchez, C. Pablos and R. van Grieken, Understanding the effect of morphology on the photocatalytic activity of TiO_2 nanotube array electrodes, *Electrochim. Acta*, 2016, **191**, 521–529.

[31] S. A. Hameed, Photo-Degradation of Vat Dye by Bimetallic Photo-Catalysts (Cu-Ni/ TiO_2 and Cu-Ni/ Zno) Under UV and Visible Light Sources, *IOSR J. Environ. Sci.*, 2016, **10**, 1–05.

[32] Y. Suyama, M. Otsuki, S. Ogisu, R. Kishikawa, J. Tagami, M. Ikeda, H. Kurata and T. Cho, Effects of light sources and visible light-activated titanium dioxide photocatalyst on bleaching., *Dent. Mater. J.*, 2009, **28**, 693–9.